A sub-circuit MOSFET model with a wide temperature range including cryogenic temperature*

Jia Kan(贾侃)†, Sun Weifeng(孙伟锋), and Shi Longxing(时龙兴)

National ASIC System Engineering Research Center, Southeast University, Nanjing 210096, China

Abstract: A sub-circuit SPICE model of a MOSFET for low temperature operation is presented. Two resistors are introduced for the freeze-out effect, and the explicit behavioral models are developed for them. The model can be used in a wide temperature range covering both cryogenic temperature and regular temperatures.

Key words: SPICE model; low temperature; sub-circuit; freeze-out effect; voltage control resistor
DOI: 10.1088/1674-4926/32/6/064002 **EEACC:** 2570

1. Introduction

The operation of a MOSFET at cryogenic temperatures has considerable improved performance: larger carrier mobility and saturation velocity, smaller sub-threshold slope, better reliability, etc. Consequently, the application of a MOSFET at cryogenic temperature has become very popular, such as infrared focal plane arrays, and detectors in the national defense and outer space areas[1−4]. As CAD engineering has become more and more important, it is necessary to have an exact MOSFET SPICE model under a cryogenic temperature environment.

Although the requirements of a low temperature MOSFET SPICE model are clear, regular MOSFET models cannot reproduce the low temperature character of a MOSFET properly. Actually, although there has been much research on the character and operation of MOSFETs at low temperature[5−7], and many analytical and numerical models that emphasize this academic study have been developed[8−11], there is no standard SPICE model for cryogenic temperature operation of a MOSFET yet. A convenient solution of this problem is a sub-circuit model, which is available to achieve good accuracy and compatibility with various SPICE simulators. In Refs. [12, 13], sub-circuit models for liquid nitrogen temperature have been reported, although both of them can be used under a fixed temperature only. In addition, since the model in Ref. [12] is constructed as polynomial functions, it is likely to result in a convergence problem during simulation.

In this paper, a sub-circuit model with a wide temperature range from cryogenic temperatures to regular temperatures (77–300 K) is developed. Two resistors are introduced for the freeze-out effect, and the explicit expression of them is developed according to the measurement data. To reproduce the low temperature characterization accurately, the effects of MOSFET node voltages V_{gs}, V_{ds}, and V_{bs} on the two resistors are all taken into consideration.

2. Problems of regular MOSFET models under low temperature

For most regular MOSFET models, they are assumed to be used in the normal temperature range, and the doping is assumed to be 100% ionized. However, when the temperature is extremely low, the ionization of doping will be significantly lowered. This is the so called “impurity freeze-out effect”. Although the cryogenic temperature environment affects MOSFET characteristic in many aspects, the impurity freeze-out effect created the most difficulty for regular MOSFET model to get a good fit.

The measurement data of a MOSFET at 77 K and the corresponding fitting curves with BSIM3v3 are shown in Fig. 1. For the effect of impurity freeze-out, it is found that when V_{ds} and/or V_{gs} are small, I_{ds} is restrained, which makes it impossible for the regular MOSFET model (BSIM3v3) to get accurate simulation result in the whole bias conditions. In particular, from the g_{ds} curves in Fig. 1(c), the impurity freeze-out effect can be clearly observed, and BSIM3v3 apparently fails to reproduce the freeze-out effect.

3. Low temperature modeling

3.1. Analysis of the freeze-out effect modeling

In our model, the outside sub-circuit part is added on a regular MOSFET model for the freeze-out effect. To make it cover a wide range from cryogenic temperatures to room temperature, the outside sub-circuits part should be effective only when the freeze-out effect exists; when the temperature rises, the effect of the outside sub-circuit model degenerates and the entire model comes to the original model. For the regular model, which should be used as the core of the sub-circuit model, we select BSIM3v3 in this paper.

The freeze-out effect changes the character of the MOSFET by two mechanisms: one is the impurity freeze-out effect in the lightly doped drain (LDD) structures, which is a function of the lateral electric field in this region; another is chan-

* Project supported by the Natural Science Foundation of Jiangsu Province, China (No. BK2008287) and the Advanced Research of National Natural Science Foundation of Southeast University, China (No. XJ2008312).
† Corresponding author. Email: jiakan.01@gmail.com
Received 15 December 2010, revised manuscript received 14 February 2011

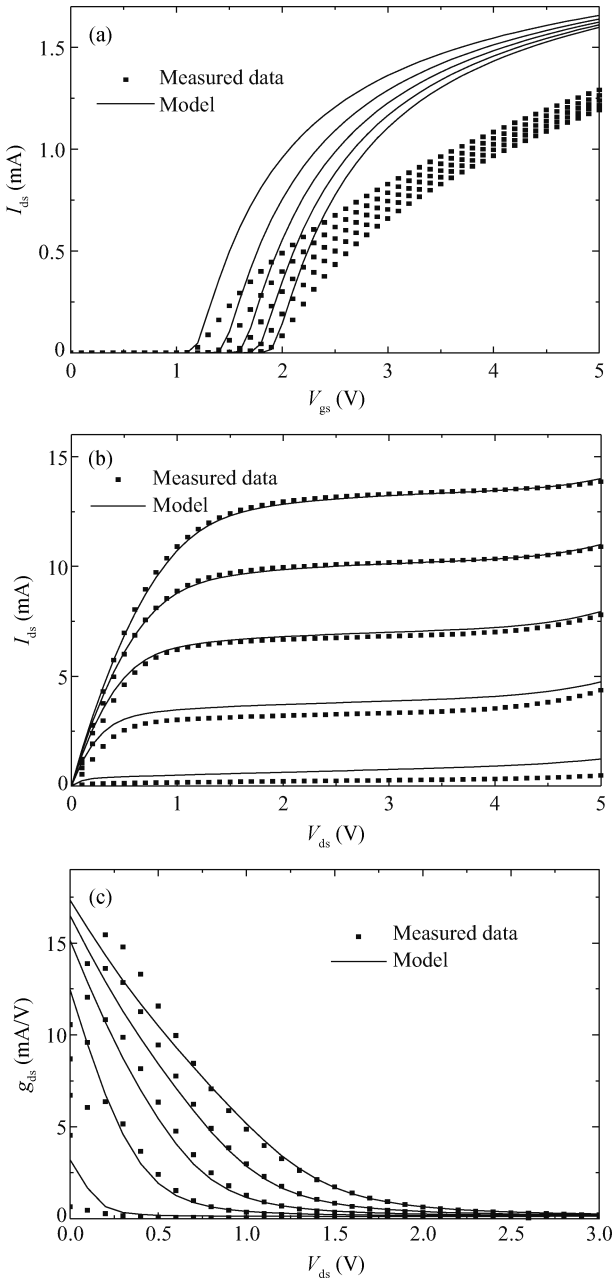

Fig. 1. MOSFET measurement data (NMOS, $W/L = 20\ \mu$m/0.5 μm) in 77 K environment and fitting curves with BSIM3v3 model. (a) I_{ds} as a function of V_{gs} for different V_{bs} at $V_{ds} = 0.1$ V. (b) I_{ds} as a function of V_{ds} for different V_{gs} at $V_{bs} = 0$ V. (c) g_{ds} as a function of V_{ds} for different V_{gs} at $V_{bs} = 0$ V.

nel impurity freeze-out, which is mainly affected by the transverse electric field (vertical to the current flow direction). Any changes to the node voltages (V_{gs}, V_{ds}, and V_{bs}) can affect the electric field, then the electric field dependence of the freeze-out can be concluded as the dependence on device node voltages. So for our sub-circuit model, it would be necessary to include the dependence on node voltages (V_{gs}, V_{ds}, and V_{bs}).

3.2. Basic sub-circuit structure

To model the impurity freeze-out effect, two voltage control resistors (R_d, R_s) are added on a BSIM3v3 core, which is shown in Fig. 2. R_d is added to account for the freeze-out

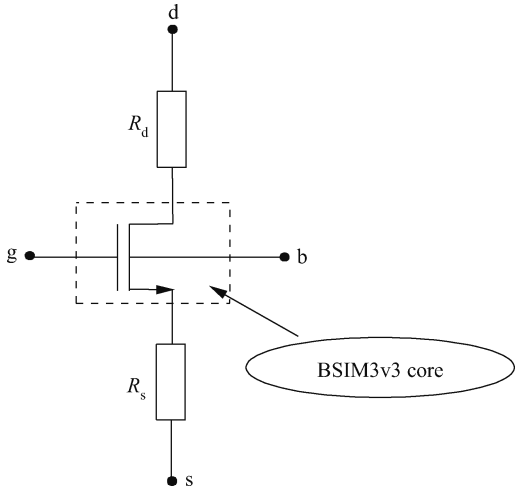

Fig. 2. Basic sub-circuit structure with resistors R_d and R_s.

effect in the LDD region, and R_s accounts for the freeze-out effect in the channel region. All of them are dependent on the temperature and node voltages (V_{ds}, V_{gs}, and V_{bs}).

3.3. R_d and R_s modeling

3.3.1. Temperature dependence modeling

R_d and R_s are introduced to account for the impurity freeze-out effect, which means that the doping cannot be assumed as 100% ionized. In Ref. [14], the resistance accounting for the impurity ionization process is expressed as

$$R_{d/s} = R_{min} \cdot (N_d/N_d^+), \tag{1}$$

where R_{min} is the original resistance without the freeze-out effect, N_d is the impurity concentration, and N_d^+ is the ionized impurity concentration. N_d^+/N_d is the fraction of ionized impurities, which is dependent on the temperature. In our sub-circuit model, since R_{min} has already been included in the BSIM3v3 core model, we remove it from $R_{d/s}$, so Equation (1) becomes

$$R_{d/s} = R_{min} \cdot (N_d/N_d^+ - 1). \tag{2}$$

According to Eq. (2), to get the value of $R_{d/s}$, N_d^+ should be calculated first. However, the temperature dependence of N_d^+ is very complicated. For the regular temperature range, we have $N_d^+ \approx N_d$ and $R_{d/s} \approx 0$; for low temperatures with the impurity freeze-out effect, N_d^+ can be expressed as[15]

$$N_d^+ = \left(\frac{N_c N_d}{2}\right)^{1/2} \exp\frac{E_d E_c}{2kT}, \tag{3}$$

where N_c is the effective density of states of the conduction band, E_d is the donor energy level, E_c is the energy level of the bottom of the conduction band, k is the Boltzmann constant, and T is the system temperature.

For low temperatures with the impurity freeze-out effect, $R_{d/s}$ can be calculated according to Eqs. (2) and (3). However, Equations (2) and (3) become invalid for the regular temperature range, which means that they are not suitable for our sub-circuit model.

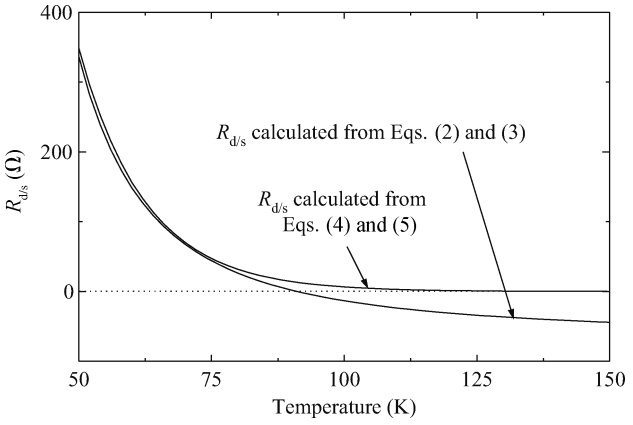

Fig. 3. $R_{d/s}$ calculated from Eqs. (2) and (3). $R_{d/s}$ calculated from Eqs. (4) and (5).

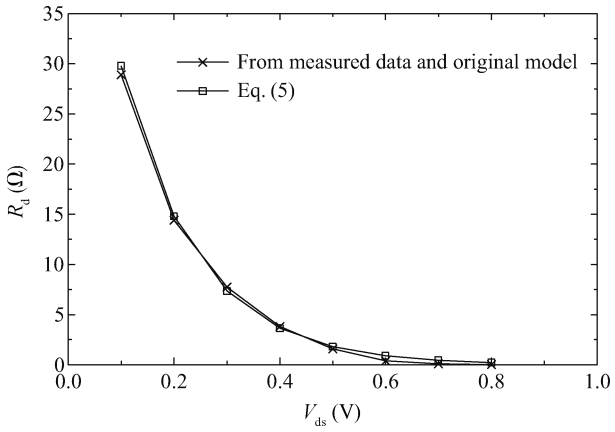

Fig. 4. Value of R_d calculated by measured data and original model. The value of R_d is calculated according to Eq. (5).

To obtain the value of $R_{d/s}$ in a wide temperature range covering both cryogenic temperatures and regular temperatures, a new expression of $R_{d/s}$ is employed in our sub-circuit model,

$$R_d = R_{d0} \exp\left(\frac{-\text{temp}}{\text{pt}}\right), \tag{4}$$

or

$$R_s = R_{s0} \exp\left(\frac{-\text{temp}}{\text{pt}}\right), \tag{5}$$

where temp is the system temperature on the Kelvin scale, $R_{d0}(R_{s0})$ can be seen as the value of $R_d(R_s)$ at 0 K, and pt is the only model parameter for the temperature dependence of R_d and R_s. Equations (4) and (5) are compared with Eqs. (2) and (3) in Fig. 3.

As shown in Fig. 3, for the low temperature range, the result of our new $R_{d/s}$ expression is very close to the result from Eqs. (2) and (3). When the temperature rises, Equation (3) becomes invalid and we get a negative $R_{d/s}$ value from it; on the other hand, the result of our new $R_{d/s}$ expression for risen temperature is $R_{d/s} \approx 0$, which is similar to the actual situation according to our analysis before. Therefore, our new $R_{d/s}$ expression keeps its validity over a wide range from cryogenic temperature to room temperature.

3.3.2. Voltage dependence modeling

Consider R_d first. With the given temperature, R_d is dependent on node voltages (V_{ds}, V_{gs} and V_{bs}). The dependence of R_d on node voltage V_{ds} can be found with the measurement data under cryogenic temperature and the simulation data with a proper original core BSIM3v3 model. As shown in Fig. 2, by assuming $R_s = 0$, with a proper original core BSIM3v3 model, R_d can simply be calculated according to the following relationship, $R_d = (V_{ds,m} - V_{ds,BSIM})/I_{ds,m}$, where $V_{ds,m}$ and $I_{ds,m}$ are from the actual measured data, and $V_{ds,BSIM}$ is the drain–source voltage of the BSIM3v3 core when $I_{ds,BSIM} = I_{ds,m}$. With this method, the value of R_d is calculated according to measured data and the original core BSIM3v3 model, as shown in Fig. 4.

According to Fig. 4, R_d has a strong dependence on V_{ds}. When V_{ds} is small, R_d is a considerable value that cannot be ignored; when V_{ds} becomes bigger, R_d decreases very quickly. In order to model the V_{ds} dependence of R_d, as shown in Fig. 4, the variable R_{d0} in Eq. (4) is replaced as a node voltage dependent function, which is expressed as

$$R_{d0} = \frac{\text{Prd0}}{W} e^{-\text{Ppd0}\cdot V_{ds}}, \tag{6}$$

where Prd0 and Ppd0 are model parameters accounting for the V_{ds} dependence of R_{d0}, and W is the channel width of the MOSFET, which is introduced for better scalability of the sub-circuit model. The result R_d with Eq. (5) is also shown in Fig. 4. As shown in Fig. 4, Equation (5) is compared with the value of R_d calculated according to measured data and the original core BSIM3v3 model, which indicate that Equation (5) achieves good accuracy of R_d.

However, the freeze-out effect is also affected by V_{gs} and V_{bs}. To get a better fitting result, V_{gs} and V_{bs} dependences for R_d are added to our newly developed R_d model with an empirical method. To introduce V_{gs} dependence, Prd0 and Ppd0 in Eq. (5) are replaced by functions of V_{gs}, and Equation (5) is modified as

$$R_{d0} = \frac{1}{W}(\text{prd0} + \text{prdg}\cdot V_{gs} + \text{prdg1}\cdot V_{gs}^2) e^{-(\text{ppd0}+\text{ppdg}\cdot V_{gs})V_{ds}}. \tag{7}$$

In Eq. (6), Prd0 is replaced by (prd0 + prdg·V_{gs}+ prdg1·$V_{gs}{}^2$); Ppd0 is replaced by (ppd0 + ppdg·V_{gs}); and both of them become functions of V_{gs}. In Eq. (6), prd0, prdg, prdg1, ppd0, and ppdg are model parameters, prd0 and ppd0 are introduced to take care of the V_{ds} dependence of the freeze-out effect; and prdg, prdg1, and ppdg are introduced to account the V_{gs} dependence of the freeze-out effect.

As the last step, V_{bs} dependence is introduced for R_{d0} function, and Equation (6) is modified to

$$R_{d0} = \frac{1}{W}\left[\text{prd0} + \text{prdg}(V_{gs} - \text{prb0}\cdot V_{bs}) + \text{prdg1}\ (V_{gs} - \text{prb0}\cdot V_{bs})^2\right] e^{-(\text{ppd0}+\text{ppdg}\cdot V_{gs})V_{ds}}. \tag{8}$$

prb0 is the model parameter that was introduced to take care of the dependence of R_{d0} on V_{bs}. After this modification, with Eqs. (4) and (7), the final expression of R_d is completed.

Table 1. All of the parameter values of our sub-circuit model.

para	(o)para	lpara	wpara	ppara
pt	60	0	0	0
prd0	691.09146	8.51941×10^{-2}	2.450215×10^{-3}	-1.569387×10^{-6}
prdg	1.479858×10^{3}	-1.906×10^{-3}	0	-6.48×10^{-9}
prdg1	–186.566723	1.019089×10^{-4}	0	1.11702×10^{-9}
ppd0	14.196826	-3.628186×10^{-6}	0	$-9.204412 \times 10^{-13}$
ppdg	–2.446277	1.200869×10^{-6}	0	1.240918×10^{-12}
prb0	0.320492	-1.84×10^{-7}	1.507937×10^{-7}	-9×10^{-14}
prs0	7366.587	0.49376	1.011042	-7.9894×10^{-7}
prsg	2.173915	1.487414×10^{-7}	-5.484208×10^{-7}	0
prb1	–0.373859	1.134189×10^{-7}	1.019439×10^{-7}	0

R_s is introduced to account for the freeze-out effect in the channel region. The difference between R_d and R_s is that R_d accounts for the freeze-out effect when V_{ds} is small, whereas R_s accounts for the freeze-out effect when V_{ds} is small. With a similar method as R_{d0} development above, the expression of R_{s0} is developed as

$$R_{s0} = \frac{L}{W} \cdot \text{prs0} \cdot \text{e}^{-\text{prsg}(V_{gs}-\text{prb1}\cdot V_{bs})}, \quad (9)$$

where L is the channel length of the MOSFET, and prs0, prsg, and prb1 are model parameters. An exponential function is selected for R_{s0}, which is developed empirically according to the measured data with the same method as R_{d0}.

3.4. Scalable

To enhance the scalability of our sub-circuit model for devices with different dimensions, model parameters introduced above can be binned follow this implementation,

$$\text{para} = \text{para0} + \text{lpara}/L + \text{wpara}/W + \text{ppara}/(LW). \quad (10)$$

For example, for the parameter pt: $\text{pt} = \text{pt0} + \text{lpt}/L + \text{wpt}/W + \text{ppt}/(LW)$. All parameters introduced in our sub-circuit model are binable.

4. Model verification and discussion

With the sub-circuit in Fig. 2 and Eqs. (4), (5), (8) and (9), the whole sub-circuit model is completed. Apart from the BSIM3v3 core, 10 parameters are added for the special characteristics of the MOSFET under cryogenic temperature. The model has been verified by fitting MOSFET characteristics for a 0.5 μm CMOS process. This process makes use of a gate oxide thickness t_{ox} of 12.5 nm and a supply voltage V_{dd} of 5 V. The model is capable of covering all length/width ranges of the device. With the temperature dependence added for the sub-circuit model, it can be used in a wide temperature range covering both cryogenic and regular temperatures.

Parameters of the BSIM3v3 core should be extracted first. In this step, besides measurement data under the regular temperature range (–40 to 125 ℃), the measurement data under 77 K should also be taken into account. Without an accurate BSIM3v3 core model, it is impossible to get an accurate fitting under cryogenic temperature.

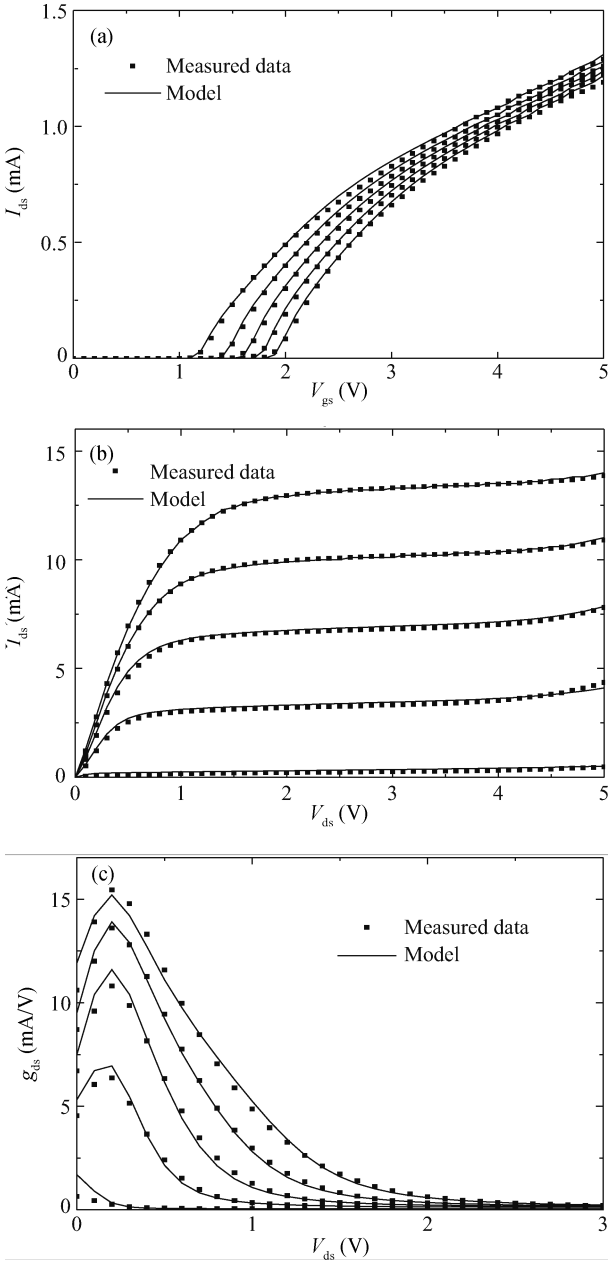

Fig. 5. MOSFET measurement data (NMOS, $W/L = 20\ \mu$m/0.5 μm) in a 77 K environment and fitting curves with the new sub-circuit model. (a) I_{ds} as a function of V_{gs} for different V_{bs} at $V_{ds} = 0.1$V. (b) I_{ds} as a function of V_{ds} for different V_{gs} at $V_{bs} = 0$ V. (c) g_{ds} as a function of V_{ds} for different V_{gs} at $V_{bs} = 0$ V.

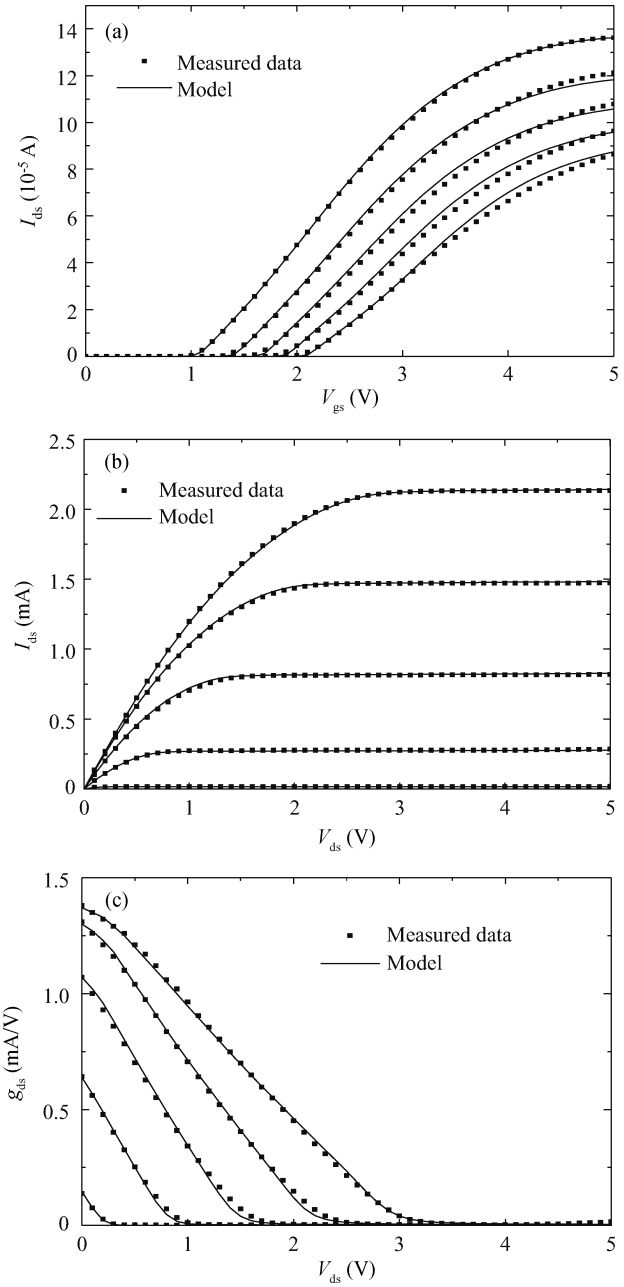

Fig. 6. MOSFET measurement data (NMOS, $W/L = 20\ \mu$m/20 μm) in a 77 K environment and fitting curves with the new sub-circuit model. (a) I_{ds} as a function of V_{gs} for different V_{bs} at $V_{ds} = 0.1$ V. (b) I_{ds} as a function of V_{ds} for different V_{gs} at $V_{bs} = 0$ V. (c) g_{ds} as a function of V_{ds} for different V_{gs} at $V_{bs} = 0$ V.

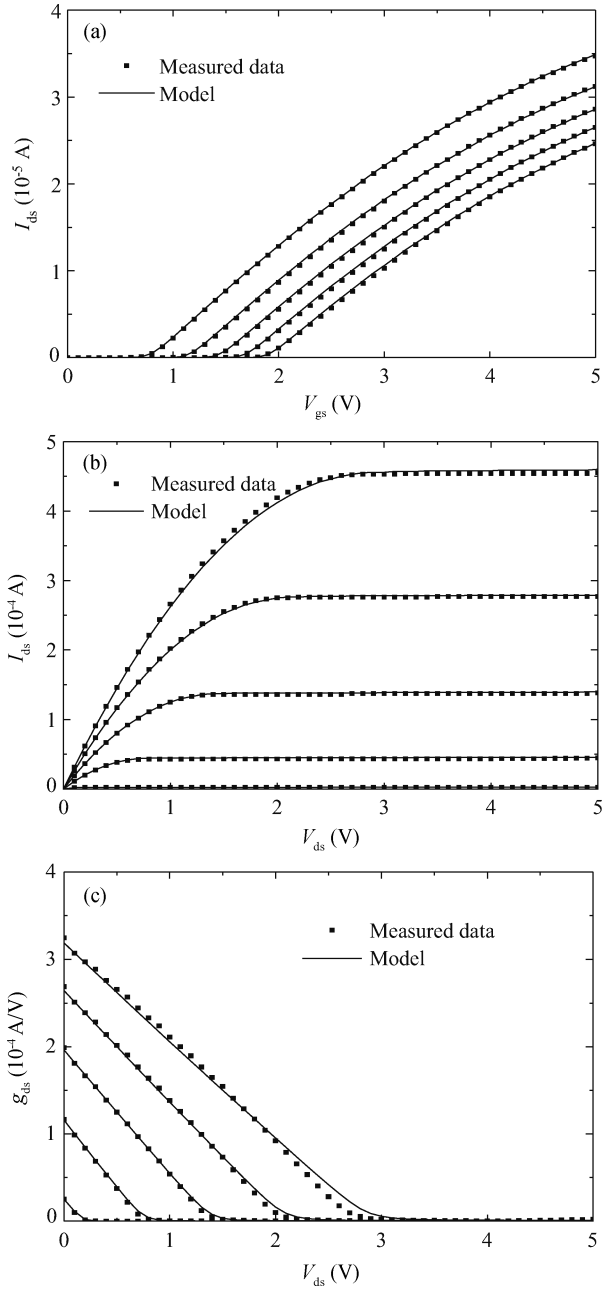

Fig. 7. MOSFET measurement data (NMOS, $W/L = 20\ \mu$m/20 μm) in a 25 ℃ environment and fitting curves with the new sub-circuit model. (a) I_{ds} as a function of V_{gs} for different V_{bs} at $V_{ds} = 0.1$ V. (b) I_{ds} as a function of V_{ds} for different V_{gs} at $V_{bs} = 0$ V. (c) g_{ds} as a function of V_{ds} for different V_{gs} at $V_{bs} = 0$ V.

After extraction of the core model, the R_d/R_s parameters of the sub-circuit can be extracted with measurement data under 77 K. With the present R_d/R_s parameters and a proper BSIM3v3 core model, an accurate fitting result can be reached. All extracted parameter values of our sub-circuit model are listed in Table 1.

As shown in Table 1, binned parameters are also extracted according to the measurement data with different device dimensions. Due to the good scalability of our sub-circuit model, this set of parameter values in Table 1 can be used for devices with various dimensions. The fitting curves of devices with the parameter values in Table 1 are presented in Figs. 5–7.

In Fig. 5, I_{ds}–V_{gs}, I_{ds}–V_{ds}, and g_{ds}–V_{ds} curves are shown for the device of $W/L = 20\ \mu$m/0.5 μm under –196 ℃. By comparison of Fig. 5 and Fig. 1, the improvement in our model compared with the BSIM3v3 model is considerable. In Fig. 6, fitting curves of devices with different dimensions are shown, which indicate the good scalability of the new sub-circuit model. Figure 7 shows the fitting curves of the device in a 25 ℃ environment with the new sub-circuit model. As described in the previous sections, the effect of the outside sub-circuit model degenerate and the model still achieves good accuracy.

5. Conclusion

Based on a physical analysis of MOSFET operation in a cryogenic temperature environment, a sub-circuit model has been presented. Two voltage control resistors have been developed for modeling the freeze-out effect. The temperature dependence is added for a wide temperature range covering both cryogenic and regular temperature ranges. In terms of the model verifications with the actual MOSFET measured data, the suggested model can provide an accurate description for both cryogenic and regular temperatures.

References

[1] Foty D. An evaluation of deep-submicron CMOS design optimized for operation at 77 K. Industrial Electronics, ISIE, 2005: 1139

[2] Xu J, Cheng M C. Design optimization of high-performance low-temperature 0.18 μm MOSFETs with low-impurity-density channels at supply voltage below 1 V. IEEE Trans Electron Devices, 2000, 47(4): 813

[3] Haldar P, Ye H, Efstathiadis H, et al. Improving performance of cryogenic power electronics. IEEE Trans Components, Applied Superconductivity, 2005, 15(2): 2370

[4] Cretu B, Balestra F, Ghibaudo G. Low temperature operation of ultra-thin gate oxide sub-0.1 μm MOSFETs. Proceedings of the 5th European Workshop on Low Temperature Electronics, 2002: 57

[5] Clark W F, El-Kareh B, Pires R G. Low temperature CMOS—a brief review. IEEE Trans Components, Hybirds, and Manufacturing Technology, 1992, 15(3): 397

[6] Ghibaudo G, Balestra F. Low temperature characterization of silicon CMOS devices. Microelectron Reliab, 1997, 37(9): 1353

[7] Balestra F, Ghibaudo G. Brief review of the MOS device physics for low temperature electronics. Solid State Electron, 1994, 37(12): 1967

[8] Pieper R J, Michael S. Comprehensive analytical approach to predicting freeze-out and exhaustion for uniform single-impurity semiconductors in equilibrium. IEEE Trans Education, 2005, 48(3): 413

[9] Briglia F, Ho F D. Device modeling for MOS devices at low temperatures. IEEE Proc Southeastcon, 1991, 1: 378

[10] Ghazavi P, Ho F D. Two-dimensional MOS device modeling at low-temperature. IEEE Proc Southeastcon, 1992, 1: 189

[11] Ghazavi P, Ho F D. A numerical model for MOSFET's from liquid-nitrogen temperature to room temperature. IEEE Trans Electron Devices, 1995, 2(1): 123

[12] Yi Yangbo, Ge Zhe, Li Haisong, et al. Modeling and parameters extraction technique for the MOSFETs at liquid nitrogen temperature. Chinese Journal of Electronics, 2009, 18(2): 215

[13] Liu Wenyong, Ding Ruijun, Feng Qi. SPICE model for LDD structure CMOS device at 35 K. J Infrared Millim Waves, 2008, 27(6): 465

[14] Hafez I M, Ghibaudo G, Balestra F, et al. Impact of LDD structures on the operation of silicon MOSFETs at low temperature. Solid-State Electron, 1995, 38(2): 419

[15] Sapoval B, Hermann C, Hermann C. Physics of semiconductors. Springer, 2003